Evanescent states in two-dimensional electron systems with spin-orbit interaction and spin-dependent transmission through a barrier

Vladimir A. Sablikov and Yurii Ya. Tkach

Kotel'nikov Institute of Radio Engineering and Electronics, Russian Academy of Sciences, Fryazino, Moscow 141190, Russia

We find that the total spectrum of electron states in a bounded two-dimensional electron gas with spin-orbit interaction contains two types of evanescent states lying in different energy ranges. The first-type states fill in a gap, which opens in the band of propagating spin-splitted states if tangential momentum is nonzero. They are described by a pure imaginary wave vector. The states of second type lie in the forbidden band. They are described by a complex wave vector. These states give rise to unusual features of the electron transmission through a lateral potential barrier with spin-orbit interaction, such as an oscillatory dependence of the tunneling coefficient on the barrier width and electron energy. However, of most interest is the spin polarization of an unpolarized incident electron flow. Particularly, the transmitted electron current acquires spin polarization even if the distribution function of incident electrons is symmetric with respect to the transverse momentum. The polarization efficiency is an oscillatory function of the barrier width. Spin filtering is most effective if the Fermi energy is close to the barrier height.

PACS number(s): 73.20.−r, 72.25.Hg, 73.43.Jn, 85.75.−d

I. INTRODUCTION

The spin-orbit interaction (SOI) in low-dimensional structures attracts a great deal of interest since it opens up the possibility of manipulating the electron spin in nonmagnetic structures using electrical means.[1,2] In this view, semiconductor heterostructures with two-dimensional (2D) electrons are very promising since the Rashba SOI is effectively controlled[3–5] by varying the applied bias or gate voltages. In recent years, predominant interest was paid to effects appearing when the SOI modifies propagating electron modes with energy above the conduction band bottom. It suffices to mention the spin-Hall effect[6–8] or spin manipulation in strained semiconductors.[9] In this paper, we show that interesting effects of the SOI arise also when the electron energy is lower than or near the conduction band bottom and evanescent states are involved. These states determine electron tunneling. They are important in 2D structures with laterally inhomogeneous potential landscape. We find that such structures can effectively polarize the transmitted electron current.

Three-dimensional (3D) tunnel structures, in which spin polarization arises due to the SOI, were considered in a number of recent works. Zakharova *et al.*[10] studied the interband tunneling. Voskoboynikov *et al.*[11] considered tunnel structures with the Rashba SOI at the interfaces. In these cases, the electron flow acquires a spin polarization if the structure, is asymmetric. In symmetric tunnel structures, the spin polarization arises if the barrier material is non-centrosymmetrical.[12] The polarization mechanism proposed by Perel' and co-workers[12,13] consists in a spin-dependent renormalization of the electron effective mass owing to the Dresselhaus SOI in the barrier. However, all these structures have a common property restricting their capability to generate spin polarization. The polarization is absent if the electron current is perpendicular to the barrier. In other words, for the spin polarization to appear, the momentum distribution function of incident electrons must be asymmetric with respect to the momentum component parallel to the barrier.

The effective mass renormalization occurs if the Hamiltonian of the SOI is quadratic in longitudinal momentum. However, the dispersion relation of electrons in the presence of the SOI is generally much more complicated and, therefore, a more careful analysis of the complex band structure and evanescent states should be carried out to study the spin-dependent tunneling. In the 3D case, such calculations were recently carried out for some specific materials and qualitatively new features were found.[14–16]

2D tunnel structures are scantily studied to date. In particular, as far as we know, even the complex band structure of 2D electrons was not explored. Though the presence of evanescent states is obvious, only a few works touched upon these modes. Usaj and co-workers[17,18] attracted evanescent states to study the electron scattering at the edges of 2D samples, but the total spectrum of evanescent states was not considered. The importance of evanescent modes in quasi-one-dimensional systems in the presence of the SOI was pointed out in a number of works.[19–22]

Khodas and co-workers[23,24] studied the electron beam propagation in 2D electron gas with spatially inhomogeneous SOI. They considered the transmission through a strip, in which the SOI strength differs from that in the rest of the 2D electron gas, to show that an initially unpolarized beam splits into two beams with different spin polarizations propagating in different directions. The consideration was restricted by propagating states since only the case of uniform potential landscape was studied. Spin-dependent reflection of electrons from a lateral barrier in a 2D system was observed in InSb/InAlSb heterostructures[25] and described theoretically in Ref. 26. Silvestrov and Mishchenko[27] demonstrated the possibility of achieving spin-polarized currents in a 2D system with smooth potential barrier and spatially uniform SOI by considering propagating modes within a semiclassical approach.

In this paper, we show that a strong polarization effect appears in 2D structures when electrons pass through a lateral potential barrier, in which the SOI is stronger than that

245321-1

in the outside 2D electron gas regions (reservoirs). The polarization arises even if the electric current is normal to the barrier. The highest polarization is attained when the electron energy is close to the conduction band bottom in the barrier. In this case, the fact that the SOI effectively splits the barrier height so that some of the electrons pass through the barrier via propagating states while others do this via the evanescent modes becomes important. Since the spin and orbital degrees of freedom are coupled, rather strong spin filtering occurs.

We study the total spectrum of electron states in a 2D bounded system with SOI to find that there are two types of evanescent states. The first-type states are characterized by an imaginary longitudinal wave vector. They fill in a gap in the propagating state spectrum. The states of the second type lie in the forbidden gap. They are described by a complex wave vector. The electron tunneling through a lateral barrier with SOI via these evanescent states exhibits unusual features, such as an oscillatory behavior of the transmission coefficient with the barrier width. However, of most interest is the spin polarization of the electron current. The polarization efficiency is high enough even if the distribution function of incident electrons is symmetric with respect to the transverse momentum. We explore the polarization efficiency in a wide range of electron energy to find that most effective spin filtering occurs if the Fermi energy is close to the barrier height.

The paper is organized as follows. In Sec. II, we describe the complex band structure and total spectrum of electron states. Section III is devoted to the tunneling through a barrier with SOI. In Sec. IV, the electric and spin currents through the barrier with SOI are considered for a wide range of the Fermi energy in the reservoirs. The results obtained for the Rashba SOI are generalized to the Dresselhaus SOI in Sec. V. We summarize and conclude in Sec. VI.

II. COMPLEX BAND STRUCTURE OF A TWO-DIMENSIONAL ELECTRON SYSTEM WITH SPIN-ORBIT INTERACTION

We start by considering the total spectrum of propagating and evanescent electron states in 2D electron gas with the Rashba SOI. The Hamiltonian is[28]

$$H_R = \frac{\hbar^2}{2m}(p_x^2 + p_y^2) + \frac{\alpha}{\hbar}(p_y\sigma_x - p_x\sigma_y), \tag{1}$$

where α is the SOI constant, and σ_x, σ_y are Pauli matrices. The eigenfunctions are

$$\psi_{\mathbf{k},s} = C e^{i(k_x x + k_y y)}\begin{pmatrix} \chi_s(\mathbf{k}) \\ 1 \end{pmatrix}, \tag{2}$$

where $s = +, -$ stands for spin states, $\mathbf{k} = (k_x, k_y)$, and C is a constant. The eigenenergy $\varepsilon_{\mathbf{k},s}$ and the spin function $\chi_s(\mathbf{k})$ are defined by the following equations:

$$(\zeta_{\mathbf{k},s} - k^2)\chi_s(\mathbf{k}) - 2a(k_y + ik_x) = 0,$$

$$-2a(k_y - ik_x)\chi_s(\mathbf{k}) + (\zeta_{\mathbf{k},s} - k^2) = 0, \tag{3}$$

where $a = m\alpha/\hbar^2$ is a characteristic wave vector of SOI, $k^2 = k_x^2 + k_y^2$, and $\zeta_{\mathbf{k},s}$ is the normalized eigenenergy:

$$\zeta_{\mathbf{k},s} = \frac{2m\varepsilon_{\mathbf{k},s}}{\hbar^2}.$$

Using Eq. (3), one obtains the dispersion equation

$$(\zeta_{\mathbf{k},s} - k^2)^2 - 4a^2k^2 = 0 \tag{4}$$

and the spin function

$$\chi_s(\mathbf{k}) = 2a\frac{k_y + ik_x}{\zeta_{\mathbf{k},s} - k^2}. \tag{5}$$

Let us analyze the dispersion equation. To be specific, let us assume that the system under consideration is infinite in the y direction and has a boundary in the x direction, i.e., the system is semi-infinite or finite in the x direction. In this case, the y component of the wave vector k_y is real, while k_x is generally complex, $k_x = k_x' + ik_x''$. Dividing the real and imaginary parts of Eq. (4), we obtain an equation set determining the energy ζ as a function of k_x', k_x'', k_y and trajectories in the (k_x', k_x'') plane, along which $\zeta(k_x', k_x'', k_y)$ is real:

$$(\zeta - k'^2 + k''^2)^2 = 4a^2(k'^2 - k''^2) + 4k'^2k''^2, \tag{6}$$

$$(\zeta - k'^2 + k''^2)k'k'' = -2a^2k'k'', \tag{7}$$

where $k' + ik'' = \sqrt{(k_x' + ik_x'')^2 + k_y^2}$.

Equation (7) possesses a solution in the following cases: (i) $k' = 0$, (ii) $k'' = 0$, and (iii) $\zeta - k'^2 + k''^2 = -2a^2$ for $k', k'' \neq 0$. The first case contradicts Eq. (6), and hence cannot be realized. The second case generates two branches of the solution, which can be found after dividing the real and imaginary parts of Eq. (6):

(1) $k_x'' = 0$,

$$\zeta_{\mathbf{k},s} = -a^2 + (a \pm \sqrt{k_y^2 + k_x'^2})^2,$$

$$\chi_s(\mathbf{k}) = \pm\frac{k_y + ik_x'}{\sqrt{k_y^2 + k_x'^2}}; \tag{8}$$

(2) $k_x' = 0$, $|k_x''| < |k_y|$,

$$\zeta_{\mathbf{k},s} = -a^2 + (a \pm \sqrt{k_y^2 - k_x''^2})^2,$$

$$\chi_s(\mathbf{k}) = \pm\frac{k_y - k_x''}{\sqrt{k_y^2 - k_x''^2}}. \tag{9}$$

The third case gives one further branch:

(3) This branch is defined for k_x', k_x'' belonging to the following trajectory:

$$k_x'^2k_x''^2 + a^2(k_y^2 + k_x'^2 - k_x''^2) - a^4 = 0, \tag{10}$$

in the complex plane (k_x', k_x''). The eigenenergy and the spin function are

$$\zeta_{\mathbf{k},s} = -a^2 - \frac{k_x'^2k_x''^2}{a^2},$$

$$\chi_s(\mathbf{k}) = -a\frac{k_y - k_x'' + ik_x'}{a^2 + ik_x'k_x''}. \tag{11}$$
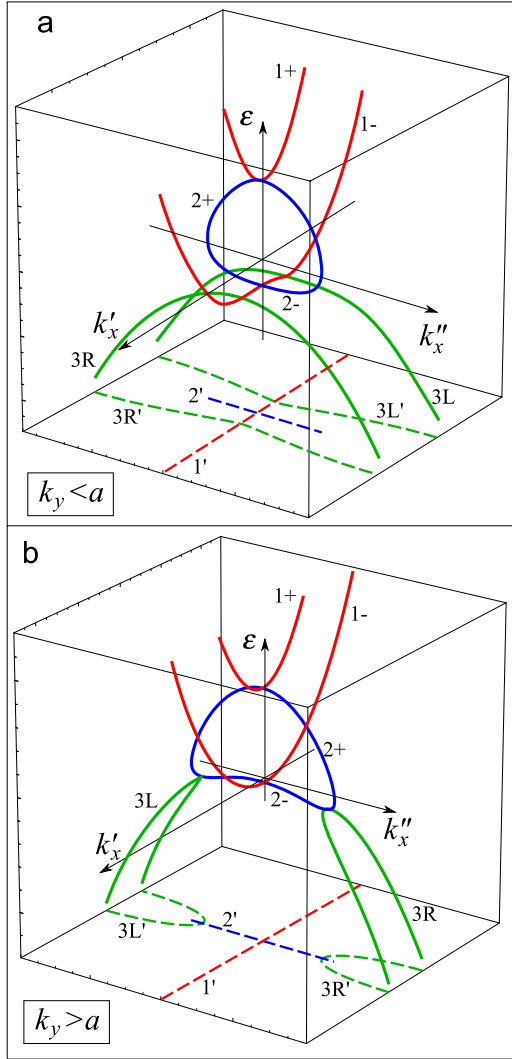
FIG. 1. (Color online) Total spectrum of 2D electron gas with SOI. Solid lines 1+ and 1− are spin-splitted propagating modes of branch 1; lines 2+ and 2− are evanescent states, branch 2; lines 3L, 3R are evanescent states in the forbidden gap, branch 3. Dashed lines 1′, 2′ and 3L′, 3R′ are the trajectories corresponding to these branches on the complex plane (k_x', k_x'').

The total spectrum is shown schematically in Fig. 1, where the energy $\varepsilon_{\mathbf{k},s}$ is presented as a function of k_x', k_x'' for a given transverse momentum k_y. The form of all three branches is different in the cases $|k_y| < a$ and $|k_y| > a$.

Branch 1 describes the propagating states with real k_x. This branch is splitted by spin. The energy gap, which opens at $k_x=0$ for $k_y \neq 0$, depends on $|k_y|$.

Branch 2 describes purely decaying evanescent states defined on the imaginary k_x axis. This branch connects the propagating state branches along the imaginary axis. The spectrum of branch 2 is also splitted by spin. The energy minimum $\varepsilon_m = -\hbar a^2/(2m)$ is common for branches 1 and 2. The minimum is attained on branch 1 if $|k_y| < a$ or on branch 2 in the opposite case.

Branch 3 corresponds to evanescent states in the forbidden gap, $\varepsilon_{\mathbf{k},s} < \varepsilon_m$. They are described by a complex longitudinal wave vector, and therefore can be named "oscillat-
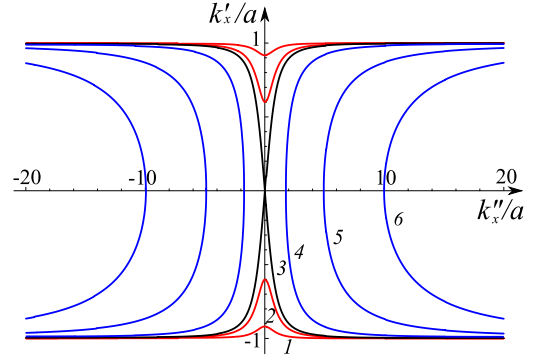

FIG. 2. (Color online) Real-energy trajectories along which the oscillating evanescent states are defined. k_y is fixed for each line: lines 1–6 correspond to $k_y/a = 0.4, 0.8, 1.0, 2.0, 5.0, 10.0$.

ing" evanescent states. The trajectories along which these states are defined obey the following equation:

$$(a^2 - k_x'^2)(a^2 + k_x''^2) = a^2 k_y^2. \tag{12}$$

They are shown in Fig. 2. There are trajectories of two types. If $|k_y| < a$, the trajectories (lines 1, 2) intersect the imaginary axis k_x''. In the vicinity of the intersection point, $|k_x''| \ll |k_x'|$ and, hence, the wave function oscillates with the distance faster than it decreases. If $|k_y| > a$, the trajectories (lines 4–6) intersect the k_x' axis.

It is seen that there are four states for any energy, in accordance with the number of the degrees of freedom of the system. At a given energy, all the states are distinguished by the wave vector components k_x', k_x'' and the spin function. The propagating states and the evanescent states of branch 2 have two sub-branches divided by the energy, while the evanescent states of branch 3 are splitted in the complex momentum plane.

Though the wave functions of the third branch are complex, they do not carry the current. Using the Hamiltonian [Eq. (1)], one obtains the following expression for the particle current in the state:

$$\psi_s = \begin{pmatrix} \psi_1 \\ \psi_2 \end{pmatrix}, \tag{13}$$

$$\mathbf{j}_s = \frac{i\hbar}{2m}(\psi_1 \nabla \psi_1^* - \psi_1^* \nabla \psi_1 + \psi_2 \nabla \psi_2^* - \psi_2^* \nabla \psi_2)$$

$$- \frac{i\alpha}{\hbar}(\psi_1 \psi_2^* - \psi_1^* \psi_2)\mathbf{e}_x + \frac{\alpha}{\hbar}(\psi_1^* \psi_2 + \psi_1 \psi_2^*)\mathbf{e}_y. \tag{14}$$

The wave functions of branch 3, calculated using Eqs. (2) and (11), are easily seen to turn the x component of the current [Eq. (14)] to zero while the y component is nonzero.

III. TUNNELING CURRENTS THROUGH A BARRIER WITH SPIN-ORBIT INTERACTION

In this section, we study the electron tunneling via the oscillating evanescent states of branch 3. Consider a 2D electron gas without SOI divided into two semiplanes (reser-

voirs) by a rectangular barrier, in which the SOI is present. The barrier height is U and the width is d.

Let us calculate the transmission probability for electrons incident on the barrier from the left reservoir. We use the presentation of the wave functions in the reservoirs in the basis of eigenstates $|s\rangle$ of the σ_z matrix. The basis functions are $|k_x, k_y, s\rangle$, where k_x and k_y are the wave vector components in the reservoirs, $s = \uparrow, \downarrow$.

In the left reservoir ($x < 0$), the wave function is

$$|\psi_{k_x,k_y,s}^{(L)}\rangle = |k_x, k_y, s\rangle + \sum_{s'} r_{s,s'} |-k_x, k_y, s'\rangle, \qquad (15)$$

where $|k_x, k_y, s\rangle$ is the state vector of incident electrons. The wave function of transmitted electrons ($x > d$) is

$$|\psi_{k_x,k_y,s}^{(R)}\rangle = \sum_{s'} t_{s,s'} |k_x, k_y, s'\rangle. \qquad (16)$$

Here, $r_{s,s'}$ and $t_{s,s'}$ are the reflection and transmission matrices.

The wave function in the barrier is expanded in the eigenstates [Eq. (2)] of the Hamiltonian [Eq. (1)]:

$$|\psi_{k_x,k_y,s}^{(B)}\rangle = \sum_{r,r'=+,-} b_{r,r'}^s |rK_x', r'K_x'', k_y\rangle, \qquad (17)$$

where $K_x = K_x' + iK_x''$ denotes the complex wave vector in the barrier; $r, r' = \pm$ are indices labeling all four evanescent states in the barrier. They are described by the spinors [Eq. (2)], in which the real and imaginary parts of K_x should be taken with different signs.

The matrices $r_{s,s'}$, $t_{s,s'}$, and $b_{r,r'}^s$ are determined by an equation set, which follows from the boundary conditions at the interfaces of the barrier and 2D electron reservoirs.

Boundary conditions for wave functions are obtained in a standard way by integrating the Schrödinger equation over the infinitesimal vicinity of the boundary. These conditions are well known for a boundary between regions with different strengths of SOI.[23,29] In our case, it is necessary to take into account that the lateral potential step at the boundary also contributes to the SOI. In the transition region, where the potential $U(x)$ varies with x, the following additional term should be added to the Hamiltonian [Eq. (1)]:

$$H_{so}^b = \frac{\gamma}{\hbar} \frac{dU}{dx} \sigma_z p_y, \qquad (18)$$

where γ is the SOI constant connected with α by $\alpha = -e\gamma F_z$, F_z being the electric field perpendicular to the 2D layer. This term, having been integrated over the transition region, gives a finite contribution to the boundary conditions. Finally, one obtains the following equations for the spinor [Eq. (13)] components:

$$\psi_1|_{-0}^{+0} = \psi_2|_{-0}^{+0} = 0; \qquad (19)$$

$$\frac{1}{m(x)} \left[\frac{\partial \psi_1}{\partial x} \pm \beta(x) k_y \psi_1 - a(x) \psi_2 \right]_{-0}^{+0} = 0, \qquad (20)$$

$$\frac{1}{m(x)} \left[\frac{\partial \psi_2}{\partial x} \mp \beta(x) k_y \psi_2 + a(x) \psi_1 \right]_{-0}^{+0} = 0, \qquad (21)$$

where the parameter

$$\beta = a \frac{2U}{eF_z} \qquad (22)$$

describes the Rashba SOI caused by the in-plane field. The upper and lower signs in Eqs. (20) and (21) correspond to the boundaries at which $U(x)$ increases or decreases with x.

Applying these boundary conditions to the system under consideration, we set $a = 0$ in the 2D electron reservoirs and keep $a \neq 0$ in the barrier. For simplicity, we ignore the difference in the effective masses of electrons in the barrier and reservoirs.

In addition, the wave vectors in the barrier and the reservoirs should be matched. The tangential components k_y must be equal. The relation of the normal components is determined by equaling the energy E of an incident electron to the electron energy in the barrier:

$$E(k_x, k_y) = U + \varepsilon(K_x, k_y, s), \qquad (23)$$

where $\varepsilon(K_x, k_y, s)$ is defined by Eqs. (8), (9), and (11), in accordance with the energy spectrum branch (1, 2, or 3), that is considered. In the present section, we restrict ourselves by branch 3.

Finally, one obtains two equation sets for the cases of the incident spin directed up and down. Each equation set contains eight equations. Dropping elementary calculations and cumbersome expressions for matrices $t_{s,s'}$, $r_{s,s'}$, and $b_{r,r'}^s$, we turn directly to the main results.

First, note that the $t_{s,s'}$ matrix obeys the following symmetry relations:

$$t_{\uparrow\uparrow}(K_x, k_y) = t_{\downarrow\downarrow}(K_x, -k_y),$$

$$t_{\uparrow\downarrow}(K_x, k_y) = -t_{\downarrow\uparrow}(K_x, -k_y). \qquad (24)$$

The particle current through the barrier is

$$j_{k_x,k_y,s} = \frac{\hbar k_x}{m} T_s(k_x, k_y), \qquad (25)$$

where T_s is the transmission coefficient, $T_s = \Sigma_{s'} |t_{s,s'}|^2$, which is the probability of an electron to tunnel with any spin in the final state. The peculiarity of the tunneling in the presence of the SOI consists in the involvement of four interfering states with different spin structures.

One of the unusual consequences of this fact is an oscillatory dependence of the tunneling coefficient on the barrier width. This feature is demonstrated in Fig. 3. The oscillations exist when the electron energy is close to the top of the third branch: $U - E_{so} - E \ll E_{so}$, where $E_{so} = \hbar^2 a^2 / (2m)$ is a characteristic energy scale of SOI. The oscillations fade away as the energy decreases deep into the forbidden band because K_x'' exceeds K_x'. The oscillations disappear also if the tangential momentum k_y goes to zero.

Figure 3 shows clearly that the barrier filters incident electrons by spin. This process depends evidently on the incident angle and the energy of electrons. Let us consider the
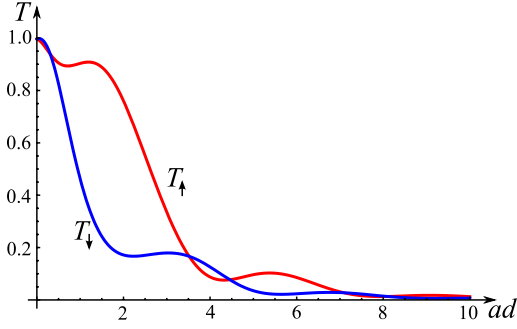
FIG. 3. (Color online) Tunneling coefficients for incident electrons with spins up and down as functions of the barrier width. $U=2E_{so}$, $E=0.95E_{so}$, $k_y=0.49a$, and $\beta=0.1$.

spin polarization of transmitted electrons in more detail. We let an unpolarized electron flow with the wave vector (k_x, k_y) incident on the barrier. The flow consists of two components $|k_x, k_y, \uparrow\rangle$ and $|k_x, k_y, \downarrow\rangle$ with opposite spins. The transmitted flow acquires spin polarization. The spin density of transmitted electrons is

$$\vec{\mu}_{k_x, k_y} = \frac{\hbar}{2} \sum_{s=\pm 1} \langle \psi^{(R)}_{k_x, k_y, s} | \hat{\vec{\sigma}} | \psi^{(R)}_{k_x, k_y, s} \rangle. \quad (26)$$

Using Eq. (16), the spin density takes the form

$$\vec{\mu}_{k_x, k_y} = \frac{\hbar}{2} |C|^2 \sum_{s, s'} [(\mathbf{e}_x - i\mathbf{e}_y s') t^*_{s, s'} t_{s, -s'} + \mathbf{e}_z s' |t_{s, s'}|^2], \quad (27)$$

where $|C|^2$ is a normalization constant.

The components of the spin polarization are shown in Fig. 4 as functions of the transverse momentum k_y for a given energy of incident electrons. The main property of the acquired polarization is that the x and z components of the spin polarization are odd functions of k_y, while the y component is an even function of k_y. This property is independent of the electron energy, the barrier height, and the SOI strength, and thus universal for the Rashba SOI. Two consequences follow from this fact. First, the unpolarized electron flow acquires spin polarization even if the distribution function of the in-
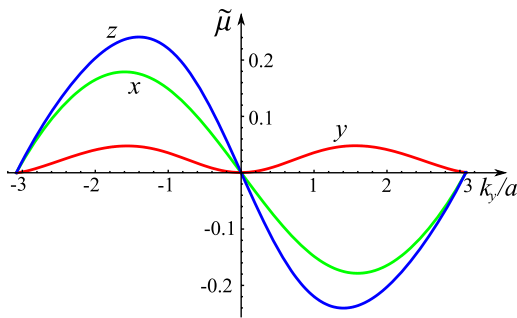

FIG. 4. (Color online) Spin polarization of transmitted electrons, $\tilde{\mu} = 2\mu_{x,y,z}/\hbar |C|^2$. The curves are marked by letters corresponding to the polarization components. The incident electron energy $E=9.5E_{so}$, the barrier height $U=11E_{so}$, the barrier width $d=a$, and the lateral SOI parameter $\beta=0.1$.
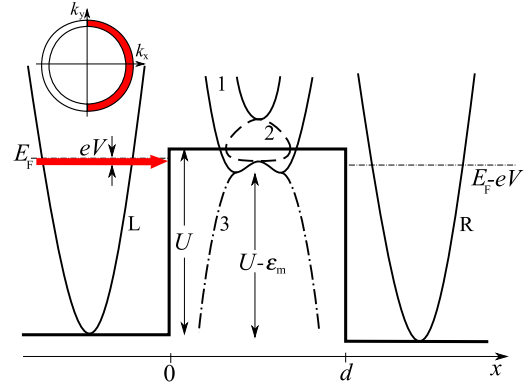

FIG. 5. (Color online) A schematic view of the barrier with SOI. Lines L and R show the electron dispersion relations in the left and right reservoirs. Lines 1, 2, 3 image schematically the corresponding branches of the dispersion relation in the barrier. The inset is the k_x, k_y space, in which the shaded region shows the electron states contributing to the current.

cident electrons is symmetric with respect to the tangential momentum direction, the polarization being directed parallel to the barrier. Second, if the distribution function is not symmetric about k_y, the spin polarization arises also in the x and z directions.

Detailed analysis shows that the spin polarization is caused mainly by the SOI in the barrier, as it is described by the Hamiltonian [Eq. (1)]. The SOI at the boundaries of the barrier [described by Eq. (18)] does not essentially affect the results if the parameter β defined by Eq. (22) is small. This case corresponds to a realistic situation in experiments. Numerical estimations for InAs quantum well ($\alpha \sim 6 \times 10^{-9}$ eV cm, $F_z \sim 10^5$ V/cm, $U \sim 20$ meV) give $\beta \sim 0.1$. If $\beta \gtrsim 1$, the boundary SOI changes the value of polarization, but the main features (such as the symmetry relations, the oscillatory behavior of the tunneling coefficients) remain qualitatively similar.

IV. SPIN POLARIZATION OF ELECTRONS BY A BARRIER WITH SPIN-ORBIT INTERACTION

In this section, we turn from the separate electron states to the total spin polarization produced by all electron states contributing to the current through a barrier with SOI. In addition, we consider a wide range of the incident electron energy to include all three branches of the electron spectrum. This allows one to find conditions under which the electron current is polarized most effectively.

Consider an electron current directed normally to the barrier. For definiteness, let the current be caused by a voltage V applied across the 2D electron reservoirs, as it is shown in Fig. 5. The incident electron states, which contribute to the current, occupy an energy layer near the Fermi level. They are located in a semiring in the k_x, k_y plane, shown in the inset. The particle and spin currents through the barrier are determined by summing over all these states. We carry out this calculation for various positions of the Fermi level E_F relative to the barrier height U to find the spin-polarization efficiency as a function of E_F.
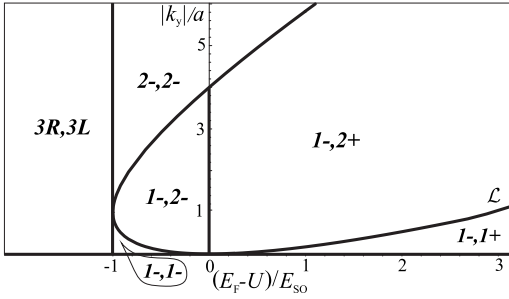
FIG. 6. The diagram of the spectrum branches accessible for electrons with energy E and tangential momentum k_y. Thick lines divide the (E,k_y) plane into six regions, in which the corresponding branches are denoted by the numbers 1, 2, 3 and chirality indices $+$, $-$, in accordance with Fig. 1. Line $\mathcal{L}$ is defined by the equation $k_y/a = (\sqrt{(E-U-E_{so})/E_{so}+1}\pm1)^2$.

For simplicity, suppose that the voltage is small compared to other energies, $eV \ll U$, E_F, E_{so}. This simplification allows one to restrict the summation by the integration in **k** space over the azimuthal angle at a given energy E. The integration is convenient to carry out over k_y, but in doing this, the fact that the set of branches, which must be used at given k_y and E, can change with varying k_y should be taken into account. This happens because the gap $\Delta\varepsilon_{12}$ between spin-split sub-branches of propagating modes (curves 1+ and 1− in Fig. 1) increases with k_y ($\Delta\varepsilon_{12} = 2\hbar^2 a|k_y|/m$) and, furthermore, the form of the dispersion curves describing the propagating $(1+,1-)$ and evanescent $(2+,2-)$ modes changes. The switches between the actual branches occur when any extremum of the dispersion curves (which is a function of k_y) coincides with the energy E. Physically, this means that electrons incident on the barrier at different angles and in different spin states feel different effective barrier heights.

Figure 6 presents a diagram showing which branches of the dispersion relation are accessible for electrons with given E and k_y. Within each region bounded by thick lines, there are two different branches with two fundamental eigenfunctions on each one or one branch with four solutions.

For each region of the diagram, the wave functions are determined in the same way as in Sec. III. The only difference is that the eigenfunctions of the branches specified in the diagram are to be used in Eq. (17) instead of the wave functions of branch 3. As a result of these calculations, the transmission $t_{s,s'}(E,k_y)$ and reflection $r_{s,s'}(E,k_y)$ matrices are obtained for the whole (E,k_y) plane. Using $t_{s,s'}(E,k_y)$, we find the particle and spin currents in the right electron reservoir.

The particle current is found by the summation of Eq. (25) over all states of incident electrons:

$$J = \frac{eV}{2\pi h} \int_{-k_F}^{k_F} dk_y (|t_{\uparrow\uparrow}|^2 + |t_{\uparrow\downarrow}|^2 + |t_{\downarrow\uparrow}|^2 + |t_{\downarrow\downarrow}|^2), \quad (28)$$

where the integration symbol implies also the summation over all regions of the (E,k_y) plane which fall within the $(-k_F,k_F)$ interval, with k_F being the Fermi wave vector in the 2D reservoirs.
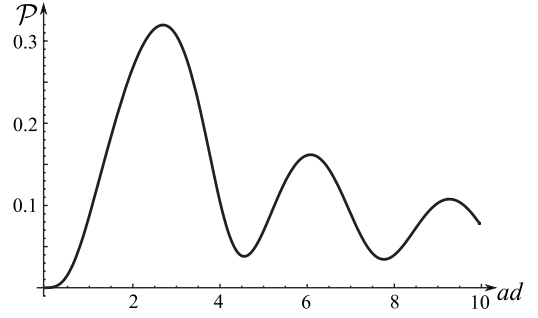

FIG. 7. Dependence of the polarization efficiency on the barrier width for the Fermi energy below E_b for tunneling through branch 3. $U=5E_{so}$, $E_F=3.5E_{so}$, and $\beta=0.1$.

The transmitted spin current in the left reservoir is defined in a standard way[30,31] using the following expression for the current in a state $|k_x,k_y\rangle$:

$$J_{s,i}^j(k_x,k_y) = \frac{1}{2}\langle v_i\sigma_j + \sigma_j v_i\rangle, \quad (29)$$

where $i=\{x,y\}$ denotes the velocity components in the plane, and $j=\{x,y,z\}$ denotes the spin components in 3D space. In the case under consideration, the x component of the total spin current is

$$J_s^j = \frac{eV}{2\pi h} \int_{-k_F}^{k_F} dk_y \begin{pmatrix} 2\,\mathrm{Re}(t_{\uparrow\uparrow}t_{\uparrow\downarrow}^* + t_{\downarrow\downarrow}t_{\downarrow\uparrow}^*) \\ 2\,\mathrm{Im}(-t_{\uparrow\uparrow}t_{\uparrow\downarrow}^* + t_{\downarrow\downarrow}t_{\downarrow\uparrow}^*) \\ |t_{\uparrow\uparrow}|^2 - |t_{\uparrow\downarrow}|^2 + |t_{\downarrow\uparrow}|^2 - |t_{\downarrow\downarrow}|^2 \end{pmatrix}, \quad (30)$$

where the three lines in the right hand side correspond to the x, y, z components of the spin polarization for the spin current directed along the x axis.

The efficiency of spin polarization is characterized by the ratio of the spin current to the particle current:

$$\mathcal{P}_j = \frac{J_s^j}{J}. \quad (31)$$

Using the symmetry relations in Eq. (24) and Eq. (30), one finds that the x and z components of the spin current are absent in the case of the Rashba SOI, and only the y component is nonzero. Of course, this is a consequence of the symmetry of the distribution function with respect to the sign of k_y. If the current were not perpendicular to the barrier, the polarization would appear also in the x and z directions. The polarization efficiency turns out to be sufficiently high. The dependencies of the polarization on the Fermi energy and the barrier width are nontrivial because they reflect a complex structure of the electron spectrum. Below, two most significant results are considered.

The dependence of $\mathcal{P}_y$ on the barrier width is shown in Fig. 7 for energies below the top of the energy band where the evanescent states of branch 3 exist in the barrier, $E_F < U - E_{so} \equiv E_b$. The polarization efficiency is seen to oscillate with d because of the interference of four oscillating evanescent modes. The effect is rather strong and becomes stronger the closer the energy is to the band top. The oscillation period is of the order of π/a.
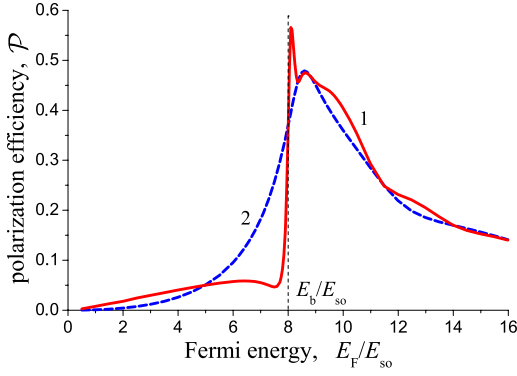
FIG. 8. (Color online) Dependence of the polarization efficiency on the Fermi energy in 2D electron reservoirs. $U=9E_{so}$ for $d=5/a$ (solid line 1) and $d=3/a$ (dashed line 2); $\beta=0.1$. Vertical dashed line marks the threshold energy $E_b=U-E_{so}$, which divides the evanescent states of branch 3 (on the left of E_b) from the states of branches 2 and 1.
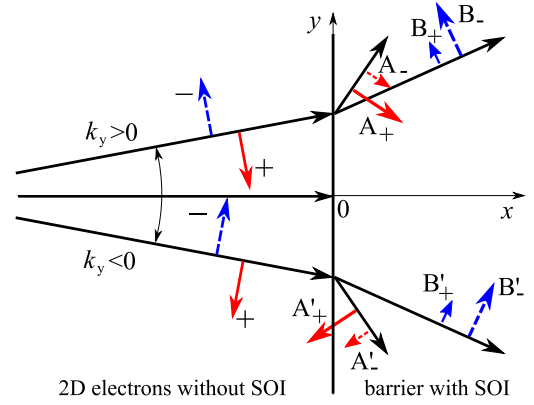

FIG. 9. (Color online) Refraction and spin polarization of electron beams incident on the semi-infinite barrier with SOI. Solid arrows show the spin polarization in the case of positive chirality of the incident beam. Dashed arrows are the polarization for negative incident chirality. $A_{\pm}$ and $B_{\pm}$ are amplitudes for incident beam with $k_y>0$. The primed letters denote the same amplitudes for $k_y>0$.

The dependence of $\mathcal{P}_y$ on the Fermi energy is presented in Fig. 8 for a wide energy range including the energy both below and above the barrier. It is seen that there is a critical energy $E=8E_{so}$, which coincides with the top energy of the third branch band, $E_b=U-E_{so}$, in the barrier. At energies well below E_b, the polarization efficiency $\mathcal{P}_y$ increases with the energy. In the vicinity of the threshold E_b, an oscillatory behavior appears as a result of the interference of four slowly decaying waves. Above this energy, the transmission process goes via the propagating states of branch 1 and the evanescent states of branch 2. At E_F slightly higher than E_b, the polarization efficiency attains the highest value. With further increasing the energy, the efficiency $\mathcal{P}_y$ decreases. It is worth noting that the highest efficiency of the spin polarization slightly depends on the SOI strength, but the barrier width at which this high polarization is attained varies inversely with the SOI constant.

Figure 8 demonstrates also how $\mathcal{P}_y$ changes with the barrier width. Increasing d above $\sim \pi/a$ leads to more pronounced oscillatory dependence of $\mathcal{P}_y$ on the energy caused by the four-wave interference.

The physical mechanism, owing to which the polarization of normally incident electron current appears, is connected with the splitting of electron waves in the barrier because of the SOI. Let us consider first a simplified case of a semi-infinite barrier region with SOI. We let the energy be high enough so that electrons occupy propagating states (branches 1+, 1−). The incident electron states can be represented in terms of two chiral modes:

$$\chi_{\pm}^{(0)} = \begin{pmatrix} \pm\chi \\ 1 \end{pmatrix}, \quad \chi = \frac{k_y + ik_x}{\sqrt{k_y^2 + k_x^2}}.$$

In the barrier region, each electron beam splits into two beams, which propagate at different angles and have different chiralities:

$$\chi_{1,2}^{(1)} = \begin{pmatrix} \chi_{1,2} \\ 1 \end{pmatrix}, \quad \chi_{1,2} = \pm\frac{k_y + iK_{1,2}}{\sqrt{k_y^2 + K_{1,2}^2}}, \qquad (32)$$

where K_1 is the x component of the wave vector of the upper mode with positive chirality χ_1 and K_2 corresponds to the lower mode with negative chirality χ_2. It is essential that $K_1<K_2$. The incident and refracted beams as well as their spin polarizations are illustrated in Fig. 9. The transmitted beam amplitudes are A_+ and B_+ for the incident beam with positive chirality, and A_- and B_- for negative chirality. The x and y components of the spin polarization in the barrier are estimated as

$$S_x \propto (|A_+|^2 + |A_-|^2)\mathrm{Re}\,\chi_1 - (|B_+|^2 + |B_-|^2)\mathrm{Re}\,\chi_2 + \cdots,$$

$$S_y \propto (|A_+|^2 + |A_-|^2)\mathrm{Im}\,\chi_1 - (|B_+|^2 + |B_-|^2)\mathrm{Im}\,\chi_2 + \cdots,$$

where the dots denote spatially dependent terms originating from the interference.

The total spin polarization is determined by the sum over all incident angles. To estimate this sum, we consider the dependence of the spin components on k_y. It is clear that $|A_{\pm}|^2$ and $|B_{\pm}|^2$ are even functions of k_y. Real and imaginary parts of $\chi_{1,2}$ are seen from Eq. (32) to be correspondingly odd and even functions of k_y. Therefore, S_x is an even function of k_y and S_y is an odd function, as illustrated in Fig. 9. Thus, the total S_x component vanishes while S_y is nonzero.

It is easy to find the direction of the total spin for the energy close to the barrier height. If $k_y=0$, the amplitudes $|A_+|$ and $|B_-|$ are equal, $|A_-|=|B_+|=0$, and $\chi_1=\chi_2=i$. Hence, the total spin density is zero because the spins of opposite chiralities cancel each other. At small k_y, the spin polarization appears. Since the amplitudes are functions of k_y^2, they remain unchanged in the first approximation, so that the resulting spin is determined by the difference $\chi_1-\chi_2$ and

$$S_y \propto \frac{K_1}{\sqrt{k_y^2 + K_1^2}} - \frac{K_2}{\sqrt{k_y^2 + K_2^2}}.$$

Since $K_1<K_2$, the y component of the spin density is negative, i.e., the sign of the spin polarization is determined by the lower-energy branch of the propagating mode.

If the barrier width is finite, there are four modes in the barrier, but the above property remains unchanged. It is also kept for other branches of the electron spectrum.

V. CASE OF DRESSELHAUS SPIN-ORBIT INTERACTION

All the above results are generalized to the case of Dresselhaus SOI. For a 2D system oriented along the [001] crystallographic direction, the SOI Hamiltonian is[32]

$$H_D = \frac{\hbar^2}{2m}(p_x^2 + p_y^2) + \frac{\alpha}{\hbar}(p_x\sigma_x - p_y\sigma_y).$$

It is well known that Dresselhaus and Rashba Hamiltonians are unitary equivalent.[33] The unitary matrix

$$U = \begin{pmatrix} 0 & i \\ 1 & 0 \end{pmatrix} \quad (33)$$

transforms the Rashba Hamiltonian [Eq. (1)] to the Dresselhaus one: $\tilde{H}_R = U^+ H_R U = H_D$. Therefore, the Dresselhaus SOI case does not require separate calculations. It is enough to carry out this transformation. Taking into account that the matrix [Eq. (33)] transforms the spin matrices as follows: $\tilde{\sigma}_x = -\sigma_y$, $\tilde{\sigma}_y = -\sigma_x$, and $\tilde{\sigma}_z = -\sigma_z$, we arrive at the following conclusions:

(i) The dispersion equation is the same as in the Rashba case [Eq. (4)].

(ii) The spin functions differ from those defined by Eq. (5) by a simple substitution $k_x \leftrightarrows k_y$.

(iii) The spin components of transmitted electrons in the incident states $|k_x, k_y, \uparrow\rangle$ and $|k_x, k_y, \downarrow\rangle$ differ from those of Sec. III by replacements $\mu_x \rightarrow -\mu_y$, $\mu_y \rightarrow -\mu_x$, and $\mu_z \rightarrow -\mu_z$.

(iv) The spin polarization of the current transmitted through a barrier with SOI has only x component if the distribution function is even with respect to the transverse momentum. In particular, Figs. 7 and 8 are valid for the spin polarization normal to the barrier, $\mathcal{P}_x$.

Of course, if the Rashba and Dresselhaus mechanisms act simultaneously, the results change qualitatively.

VI. CONCLUSION

We have found the total spectrum of electron states in a bounded 2D electron gas with SOI. It addition to well known propagating states, it contains two branches of evanescent states. Their wave functions decay with the distance in the direction x perpendicular to the boundary. One branch ("purely decaying" evanescent mode) is described by an imaginary wave vector. The energy of this state is splitted by spin, so that there are two sub-branches. They fill in the gap, which opens in the propagating state spectrum at $k_y \neq 0$. The other branch (oscillating evanescent mode) is characterized by a complex wave vector K_x. These states lie in the forbidden gap.

We have studied the electron transmission through a lateral potential barrier with the SOI. In the energy range, where electrons tunnel via the oscillating evanescent states, the tunneling reveals unusual features, such as an oscillatory dependence of the transmission coefficients on the barrier width and the energy. However, of most importance is the spin polarization of the electron current. The value and direction of the polarization depend on the angle of incidence and the energy of incident electrons. The polarization appears even if the distribution function of incident electrons is symmetric with respect to the transverse momentum. In this case, the polarization is directed parallel to the barrier (in the Rashba SOI case) or perpendicular to it (for Dresselhaus SOI). The highest efficiency of the spin polarization is attained when the Fermi energy is close to the barrier height. In this case, electrons pass through the barrier partially via the propagating states and partially via the purely decaying evanescent states. Under this condition, the most effective spin filtering occurs. The maximal polarization efficiency depends on the barrier height and can exceed 0.5 if the barrier width is on the order of π/a.

[1] *Semiconductor Spintronics and Quantum Computation*, edited by D. D. Awschalom, D. Loss, and N. Samarth (Springer, Berlin, 2002).

[2] I. Žutić, J. Fabian, and S. Das Sarma, Rev. Mod. Phys. **76**, 323 (2004).

[3] J. Nitta, T. Akazaki, H. Takayanagi, and T. Enoki, Phys. Rev. Lett. **78**, 1335 (1997).

[4] T. Matsuyama, R. Kursten, C. Meißner, and U. Merkt, Phys. Rev. B **61**, 15588 (2000).

[5] S. Schmult, M. J. Manfra, A. Punnoose, A. M. Sergent, K. W. Baldwin, and R. J. Molnar, Phys. Rev. B **74**, 033302 (2006).

[6] J. Sinova, D. Culcer, Q. Niu, N. A. Sinitsyn, T. Jungwirth, and A. H. MacDonald, Phys. Rev. Lett. **92**, 126603 (2004).

[7] O. Chalaev and D. Loss, Phys. Rev. B **71**, 245318 (2005).

[8] J. Schliemann, Int. J. Mod. Phys. B **20**, 1015 (2006).

[9] Y. Kato, R. C. Myers, A. C. Gossard, and D. D. Awschalom, Nature (London) **427**, 60 (2004).

[10] A. Zakharova, F. T. Vasko, and V. Ryzhii, J. Phys.: Condens. Matter **6**, 7537 (1994).

[11] A. Voskoboynikov, S. S. Liu, and C. P. Lee, Phys. Rev. B **58**, 15397 (1998); **59**, 12514 (1999).

[12] V. I. Perel', S. A. Tarasenko, I. N. Yassievich, S. D. Ganichev, V. V. Bel'kov, and W. Prettl, Phys. Rev. B **67**, 201304(R) (2003).

[13] S. A. Tarasenko, V. I. Perel', and I. N. Yassievich, Phys. Rev. Lett.

93, 056601 (2004).

[14] T. Sandu, A. Chantis, and R. Iftimie, Phys. Rev. B **73**, 075313 (2006).

[15] S. Mishra, S. Thulasi, and S. Satpathy, Phys. Rev. B **72**, 195347 (2005).

[16] L. G. Wang, W. Yang, K. Chang, and K. S. Chan, Phys. Rev. B **72**, 153314 (2005).

[17] G. Usaj and C. A. Balseiro, Europhys. Lett. **72**, 631 (2005).

[18] A. Reynoso, G. Usaj, and C. A. Balseiro, Phys. Rev. B **73**, 115342 (2006).

[19] M. Governale and U. Zülicke, Phys. Rev. B **66**, 073311 (2002).

[20] P. Středa and P. Šeba, Phys. Rev. Lett. **90**, 256601 (2003).

[21] M. Lee and C. Bruder, Phys. Rev. B **72**, 045353 (2005).

[22] L. Serra, D. Sánchez, and R. López, arXiv:0705.1506.

[23] M. Khodas, A. Shekhter, and A. Finkel'stein, Phys. Rev. Lett. **92**, 086602 (2004).

[24] A. Shekhter, M. Khodas, and A. M. Finkel'stein, Phys. Rev. B **71**, 125114 (2005).

[25] H. Chen, J. J. Heremans, J. A. Peters, A. O. Govorov, N. Goel, S. J. Chung, and M. B. Santos, Appl. Phys. Lett. **86**, 032113

(2005).

[26] A. O. Govorov, A. V. Kalameitsev, and J. P. Dulka, Phys. Rev. B **70**, 245310 (2004).

[27] P. G. Silvestrov and E. G. Mishchenko, Phys. Rev. B **74**, 165301 (2006).

[28] E. I. Rashba, Fiz. Tverd. Tela (Leningrad) **2**, 1224 (1960) [Sov. Phys. Solid State **2**, 1109 (1960)]; Yu. A. Bychkov and E. I. Rashba, Pis'ma Zh. Eksp. Teor. Fiz. **39**, 66 (1984) [Sov. Phys. JETP **39**, 78 (1984)].

[29] L. W. Molenkamp, G. Schmidt, and G. E. W. Bauer, Phys. Rev. B **64**, 121202(R) (2001).

[30] E. I. Rashba, Physica E (Amsterdam) **34**, 31 (2006).

[31] J. Shi, P. Zhang, D. Xiao, and Q. Niu, Phys. Rev. Lett. **96**, 076604 (2006).

[32] R. Winkler, *Spin-Orbit Coupling Effects in Two-Dimensional Electron and Hole Systems* (Springer, Berlin, 2003).

[33] E. I. Rashba and V. I. Sheka, in *Landau Level Spectroscopy*, edited by G. Landwehr and E. I. Rashba (Elsevier, Amsterdam, 1991).